

## Article

# Metal–Organic Frameworks-Derived FeCo/C–CNT Nanocomposites Modified Epoxy Resin for Electromagnetic Protection Coatings for Buildings

Dongyi Lei <sup>1,2</sup> , Jiaxin Liu <sup>1</sup>, Chengkan Liu <sup>1</sup>, Chunlei Dong <sup>1</sup>, Donglei Yang <sup>3</sup>, Ying Li <sup>1,2,\*</sup> , Jiqing Zhang <sup>4</sup>, Feizi Han <sup>5</sup> and Zihan Guo <sup>1</sup>

<sup>1</sup> School of Civil Engineering, Qingdao University of Technology, Qingdao 266520, China; leidongyi@qut.edu.cn (D.L.)

<sup>2</sup> Engineering Research Center of Concrete Technology under Marine Environment, Ministry of Education, Qingdao 266520, China

<sup>3</sup> Institute of Technical Information for Building Materials Industry, Beijing 100024, China

<sup>4</sup> Qingdao Ruiyuan Engineering Group Co., Ltd., Qingdao 266555, China; zjq20082626@163.com

<sup>5</sup> CIECC Overseas Consulting Co., Ltd., Beijing 100048, China

\* Correspondence: liying@qut.edu.cn; Tel.: +86-0532-85071133

**Abstract:** Exploring an efficient electromagnetic protection strategy for buildings is of great significance to solve the problems caused by increasing electromagnetic pollution, as the rapid progress of technology continues. In this work, FeCo alloy/carbon–carbon nanotube (FeCo/C–CNT) nanocomposites, with significant microwave absorption performance, were successfully synthesized using a simple pyrolysis method involving FeCo–ZIF MOFs precursors and added to epoxy resin to prepare a novel electromagnetic wave absorption (EWA) coating. The minimum reflection loss ( $RL_{\min}$ ) of the coating applied on the surface of the ceramic tiles was  $-23.89$  dB at 11.37 GHz and the effective absorption bandwidth (EAB) reached 8.85 GHz. Through microscopic characterization and analysis of the electromagnetic parameters of the FeCo/C–CNT nanocomposites, it was found that the EWA coating has an ultrabroad band wave absorption effect, mainly due to the comprehensive advantages of the polarization loss from CNTs, impedance matching, the dual loss synergy effect, and multiple reflection between the FeCo alloys, the carbon layer, and the CNTs. This study has successfully developed high-performance EWA materials and demonstrated the feasibility of an EWA coating applied to building surfaces, contributing to the improvement of electromagnetic protection functions of buildings.

**Keywords:** electromagnetic wave absorption; FeCo/C–CNT wave absorber; electromagnetic protection coating; metal–organic frameworks; ultrabroad band; ceramic building materials



**Citation:** Lei, D.; Liu, J.; Liu, C.; Dong, C.; Yang, D.; Li, Y.; Zhang, J.; Han, F.; Guo, Z. Metal–Organic Frameworks-Derived FeCo/C–CNT Nanocomposites Modified Epoxy Resin for Electromagnetic Protection Coatings for Buildings. *Buildings* **2024**, *14*, 1096. <https://doi.org/10.3390/buildings14041096>

Academic Editor: Ahmed Senouci

Received: 23 February 2024

Revised: 31 March 2024

Accepted: 11 April 2024

Published: 15 April 2024



**Copyright:** © 2024 by the authors. Licensee MDPI, Basel, Switzerland. This article is an open access article distributed under the terms and conditions of the Creative Commons Attribution (CC BY) license (<https://creativecommons.org/licenses/by/4.0/>).

## 1. Introduction

As information technology in society continues to advance rapidly, the widespread application of electronic equipment inevitably gives rise to electromagnetic pollution, which seriously affects human health [1–3]. The most common methods for reducing electromagnetic pollution in daily life are mainly the use of filling wave absorbers in building materials or covering the surfaces of buildings with modified electromagnetic protective coatings. Owing to the limitations in the preparation process, it remains a challenge to combine the great properties of electromagnetic wave absorption (EWA) materials with heat-resistant and oxidation-resistant characteristics when added to ceramic-based building materials [4].

EWA coatings should satisfy requirements including simple preparation, strong bonding, and high flexibility, which mainly derive from EWA materials and binders [5,6]. In general, epoxy resin is the preferred material used as a binder due to its high strength, low

density, and good chemical stability [7]. Additionally, EWA materials are mainly classified as dielectric and magnetic materials, which can effectively absorb electromagnetic energy and convert it into heat or other forms of energy for dissipation [8]. However, most traditional EWA materials still have problems including a narrow bandwidth, large thickness, and poor EWA performance [9–11]. Therefore, a high-performance microwave absorber is urgently needed.

A metal–organic framework (MOF), consisting of two parts connected by an organic ligand and a metal center, is a novel porous crystalline material that has been used in recent years. With its advantages, including a high specific surface area and an adjustable crystal structure, it has been in widespread use in the fields of gas separation, catalysis, and energy conservation [12–14]. As EWA materials, carbonized MOF materials can make up for the shortcomings of dielectric materials, such as its high permittivity and poor impedance matching, and also satisfy the wide bandwidth that is lacking in single magnetic loss materials [15,16]. The superior EWA properties of MOF-derived materials originate from its numerous pore structures and rich morphological structures. Carbonization produces carbon with abundant defects and numerous interfaces with metal particles, so the porous structure and the multiple loss mechanisms of dielectric and magnetic loss give MOF-derived materials excellent impedance and attenuation abilities [17,18]. Qin et al. [19] prepared Ni/CO@C nanocomposites with Ni, Co as the metal particles,  $\text{CH}_3\text{COONa}\cdot 3\text{H}_2\text{O}$ , and a nicotinic acid mixed solution as precursors at different temperatures, which obtained prime EWA performance at 650 °C, with a minimum reflection loss ( $\text{RL}_{\min}$ ) of  $-66.3$  dB. Wang [20] obtained CONPS/ZF-67 nanocomposites through carbonization at different temperatures, resulting in an  $\text{RL}_{\min}$  for CO/C-700 of  $-30.31$  dB at 11 GHz. Lu and colleagues [21] tuned the ratio of Co and Cu to prepare a 3D flower-shaped bimetallic nanocomposite, which reached an  $\text{RL}_{\min}$  of  $-51.7$  dB at 2.7 mm and an effective absorption bandwidth (EAB) of 6.4 GHz. Based on previous literature, we have learnt that the EWA capabilities of MOF-derived materials are higher after carbonization than before carbonization. The EWA performance of MOF-derived carbon is mainly affected by the pyrolysis temperature, which can be altered by the degree of reduction or oxidation of the metal ions and the graphitization of carbon [22,23]. For instance, LV et al. [24] attempted to obtain porous Co/C nanocomposites through carbonization at different temperatures. The  $\text{RL}_{\min}$  of Co/C-500 reaches  $-35.3$  dB in terms of an EAB of 5.80 GHz. It is well known that carbon nanotubes (CNTs) are 1D carbon materials with high electrical conductivity. Compositing CNTs with MOFs not only increases the network structure on the surface of MOFs, but also enhances its electrical conductivity, which is an effective enhancement of the EWA properties. For instance, Zhang et al. [25] obtained Co@CNT/PC composites by carbonizing ZIF-67 to grow CNTs in situ on its surface for the co-catalytic generation of CNT. Li et al. [26] prepared CoFe alloy/porous carbon@carbon nanotubes (CoFe/PC@CNTs) nanocomposites. Benefiting from the double conductive network formed between the CoFe alloy, the CNTs, and the PC, the  $\text{RL}_{\min}$  value for the CoFe/PC@CNTs nanocomposites reached  $-68.94$  dB and an EAB of 9.14 GHz at 2.63 mm. Consequently, the in situ growth of CNTs through the pyrolysis of some specific MOFs is one of the most effective strategies to develop high-performance electromagnetic wave absorbers. Nevertheless, there are fewer studies on the effect of the pyrolysis temperature on CNT growth.

In this study, FeCo alloy/carbon–carbon nanotube (FeCo/C–CNT) nanocomposites were successfully synthesized through simple pyrolysis of FeCo-ZIF MOF precursors. The effects of the microscopic morphology of the FeCo/C–CNT nanocomposites on the EWA properties at different temperatures were investigated. At 800 °C, the FeCo/C–CNT nanocomposites achieved an  $\text{RL}_{\min}$  value of  $-52.06$  dB at 13.84 GHz and an EAB value of 8.07 GHz (3.63 mm). The optimized FeCo/C–CNT nanocomposites were used as microwave absorbers, added to epoxy resin to obtain an ultrabroad band EWA coating. The coating covering the surface of the tiles obtained a minimum reflectivity of  $-23.89$  dB at 11.37 GHz and absorbed more than 90% of the electromagnetic waves in the frequency ranges 2.36–7.49 GHz and 8.55–12.27 GHz. Furthermore, the mechanisms related to the

FeCo/C–CNT nanocomposites for enhancing the EWA performance of the coating were discussed after analyzing the electromagnetic parameters. Notably, this work aims to develop a material with excellent EWA capabilities, as an ideal wave absorber, as well as to provide feasible design ideas for expanding the application of EWA coatings in the construction field.

## 2. Materials and Methods

### 2.1. Materials

Hexahydrate iron nitrate ( $\text{Fe}(\text{NO}_3)_2 \cdot 6\text{H}_2\text{O}$ , AR, >99%), cobalt nitrate hexahydrate ( $\text{Co}(\text{NO}_3)_2 \cdot 6\text{H}_2\text{O}$ , AR, >99%), and 2-methylimidazole (2-MIM, >99%) were bought from Sinopharm Chemical Reagent Co., Ltd. (Shanghai, China) The epoxy resin (E51) and curing agent (low molecular weight polyamide 650) were purchased from Qingdao Baiyi Chemical Co., Ltd. (Qingdao, China). The organic solvents xylene and N-butanol were all provided by Sinopharm Chemical Reagent Co., Ltd. (Shanghai, China). The materials in this paper were used in a direct, unpurified manner.

### 2.2. Fabrication of FeCo/C–CNT Nanocomposites

The FeCo/C–CNT nanocomposites were obtained through straightforward coprecipitation, following by pyrolysis treatment without organic solvents. In brief, 6 mmol  $\text{Fe}(\text{NO}_3)_2 \cdot 6\text{H}_2\text{O}$  and 6 mmol  $\text{Co}(\text{NO}_3)_2 \cdot 6\text{H}_2\text{O}$  were added to 40 mL of dissolved water, as solution A. In the meantime, 48 mmol 2-MIM was dissolved in 160 mL deionized water, as solution B. Solution A and B were mixed under violent agitation for 10 h. Subsequently, the precursor was collected by centrifugation, washed 3–5 times with deionized water, and then dried in a vacuum oven. Lastly, the as-prepared samples were pyrolysis treated at different temperatures, including 600, 700, and 800 °C, under  $\text{N}_2$  for 2.5 h, respectively. The final samples are defined as FeCo/C–CNT-X (X = 600, 700, and 800, respectively), where X represents the pyrolysis temperature.

### 2.3. Fabrication of Epoxy Resin Coating Modified by FeCo/C–CNT Nanocomposites

The detailed preparation process for the epoxy resin coating decorated with FeCo/C–CNT nanocomposites was as follows: Firstly, the mixture solution was prepared using xylene and N-butanol with a weight ratio of 7:3; following that the FeCo/C–CNT nanocomposites were dissolved uniformly in the solution under ultrasonic treatment. Then, the epoxy resin was preheated at 80 °C for 1 h; following that the above mixed solution was poured into the epoxy resin. Additionally, the hardener, with the same weight, was added to the epoxy resin to prepare the epoxy composite. Finally, the epoxy resin coating sample modified by FeCo/C–CNT nanocomposites was obtained, using a Teflon mold with the size  $300 \times 300 \times 2$  mm.

### 2.4. Characterization

The phase information for the specimens was gathering using X-ray diffraction patterns (XRD, Ultima IV powder diffractometer, Rigaku Inc., Tokyo, Japan). X-ray photoelectron spectroscopy (XPS, ESCALAB X1+, Thermo Fisher Scientific Inc., Waltham, MA, USA) was used to investigate the chemical components and elemental valency of the materials. Scanning electron microscopy (SEM, Sigma 500, Zeiss Group, Oberkochen, Germany and SU8010, Hitachi, Hitachi Co., Ltd., Tokyo, Japan) was conducted to analyze the morphology of the samples. Additionally, the microstructure information was studied by transmission electron microscopy (TEM, Tecnai G2 F20, Frequency Electronics Inc., Hillsboro, OR, USA). According to the coaxial line method, the microwave absorption ability of the as-prepared specimens was measured. The composites were fabricated into cylindrical specimens by mixing the samples with paraffin wax in different weight ratios. Then, the dimensions of the tested samples included an outer size of 7 mm and an inner size of 3.04 mm. The EWA performance test specimens were denoted as FeCo/C–CNT-X-Y (X = 600, 700, and 800, Y = 20, 30, and 40, respectively), where X refers to the heat-treatment temperature and Y is

the filling content. The complex permittivity ( $\epsilon_r = \epsilon' - j\epsilon''$ ) and permeability ( $\mu_r = \mu' - j\mu''$ ) of the samples were measured using a vector network analyzer (PNA-N5244A, Agilent Technologies Inc., Santa Clara, CA, USA) ranging from 1–18 GHz. The reflectance loss (RL) was measured using the complex permittivity and permeability, with the calculation equation as follows:

$$RL(\text{dB}) = 20 \log |(Z_{in} - Z_0) / (Z_{in} + Z_0)| \quad (1)$$

$$Z_{in} = Z_0 \sqrt{\mu_r / \epsilon_r} \tanh[j(2\pi f d / c) \sqrt{\epsilon_r \mu_r}] \quad (2)$$

where  $Z_0$  and  $Z_{in}$  represent the free space impedance and the input impedance of the EWA materials, respectively. Moreover,  $\mu_r$  and  $\epsilon_r$  denote the measured relatively complex permeability and permittivity, respectively. In addition,  $c$  is the speed of light,  $d$  is the thickness of the materials, and  $f$  is the frequency of the electromagnetic wave.

### 3. Results

The FeCo/C–CNT nanocomposites were fabricated by combining the coprecipitation and pyrolysis methods, as shown in the schematic diagram in Figure 1a. During the coprecipitation process, the FeCo-ZIF MOF precursor was obtained using  $\text{Fe}^{2+}$  and  $\text{Co}^{2+}$  as the metal source and 2-MIM as the organic framework. Regulating the calcination temperature, the FeCo/C–CNT nanocomposites with different lengths and contents of CNTs were synthesized. As presented in Figure 1b, the X-ray diffraction (XRD) patterns show that all the specimens have similar information. There are three diffraction peaks, namely  $44.9^\circ$  (110),  $65.3^\circ$  (200), and  $82.7^\circ$  (211), corresponding to the FeCo alloy (PDF 49-1586), respectively [27,28]. All the samples exhibit good crystallinity. The results demonstrate that the FeCo alloy was successfully prepared through carbonization [29]. However, the characteristic peaks corresponding to carbon or the CNTs were almost impossible to observe, indicating that carbon might be amorphous [30]. The peaks of FeCo/C–CNT-800 are sharper than those of FeCo/C–CNT-700 and FeCo/C–CNT-600, suggesting that an increase in temperature is more favorable to the reaction. The X-ray diffraction (XRD) patterns show that the pyrolysis temperature critically affected the phase composition of the MOF-derived composites.

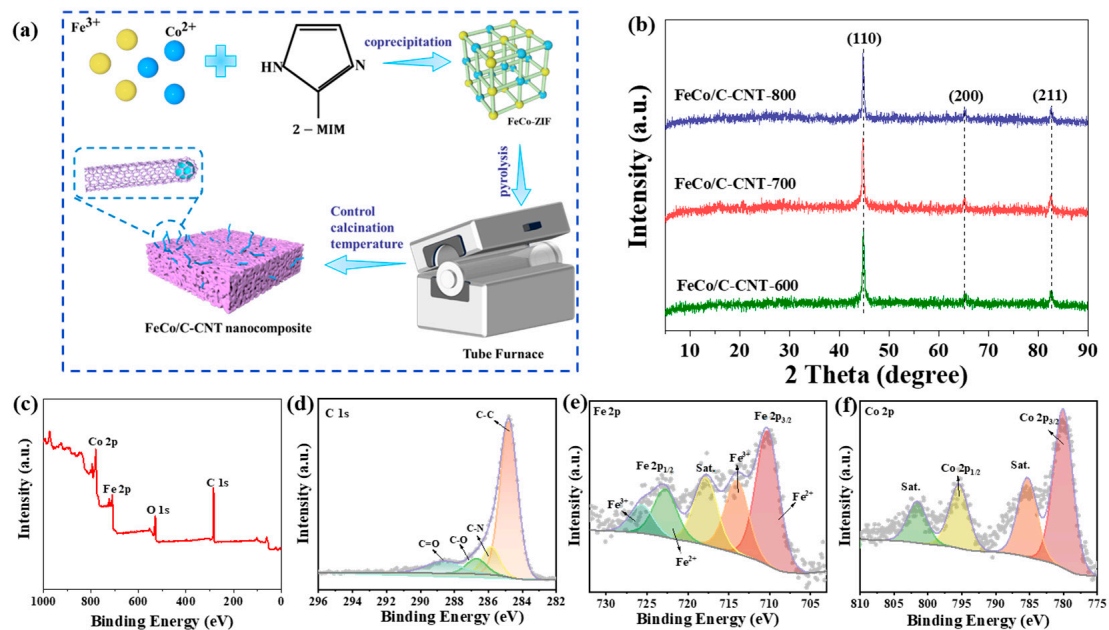


**Figure 1.** (a) Schematic illustration of the preparation process; (b) X-ray diffraction (XRD) patterns; X-ray photoelectron spectroscopy (XPS) spectra of: (c) survey spectrum, (d) C 1s, (e) Fe 2p; and (f) Co 2p of FeCo/C–CNT nanocomposites.

X-ray photoelectron spectroscopy (XPS) was conducted to accurately identify the chemical composition and surface environment of the FeCo/C–CNT nanocomposites. C, O, Fe, and Co elements can be observed in the X-ray photoelectron spectroscopy (XPS) survey spectrum (Figure 1c); where the O element might stem from the adsorbed water on the surface of the as-prepared samples. Figure 1d shows the high-resolution C 1s spectra of the FeCo/C–CNT nanocomposite; there are four peaks represented by C–C (284.84 eV), C–N (285.83 eV), C–O (286.69 eV), and C=O (88.59 eV) bonds, respectively. Figure 1e shows the Fe 2p spectrum; where Fe<sup>3+</sup> appears as the peaks at 725.58 eV and 713.62 eV, while 722.88 eV and 710.4 eV are indexed to Fe<sup>2+</sup>. The other one at 717.95 eV is a satellite peak [31]. The X-ray photoelectron spectroscopy (XPS) spectrum of Co 2p has two typical peaks belonging to Co 2p<sub>3/2</sub> (781.41 eV) and Co 2p<sub>1/2</sub> (796.76 eV), while the satellite peaks appeared at 803.82 eV and 786.87 eV [32,33]. The results are in accord with that of X-ray diffraction (XRD).

Moreover, the microscopic images, exhibited in Figure 2, are used to investigate the microstructure information of the FeCo/C–CNT nanocomposites. In Figure 2(a,a1), the FeCo-ZIF precursor displays aggregated sheet-like structures. After pyrolysis treatment, the surfaces of all the samples became rough and had a porous structure, indicating the conversion of the lamellar MOF precursor into a porous carbon skeleton. The large porous structure is conducive to improving the impedance matching of the nanocomposites, as well as prolonging the transmission path of the electromagnetic waves inside the material and increasing multiple reflection scattering. And a certain amount of the CNT is attached to the porous carbon surface, while the FeCo alloy is uniformly distributed on the surface of the porous carbon matrix and on the ends of the CNT (Figure 2(b–d1)). FeCo alloys have a particle size of about 30 nm. Notably, with the calcination temperature increase, the size and content of CNTs significantly increase. At 600 °C, while pyrolysis was not sufficient, there is less CNT being produced. The increase in temperature promotes the growth of CNTs. The formation of CNTs can originate from the transformation of highly crystallographic MOFs assembled by organic ligands as the basic units and metal clusters as the catalyst in the pyrolysis process. The CNTs present on the surface of MOF-derived porous carbon are interconnected to form a large conductive network, which is conducive to improving the conductive loss. In addition, there are a large number of interfaces between the porous carbon, the CNTs, and the FeCo alloy, which leads to more interfacial polarizations and dipole polarizations [25,34]. In addition, the energy dispersive spectrometer (EDS) mapping in Figure 2e shows that the C, O, N, Fe, and Co elements were evenly dispersed in the nanocomposite, which is in accordance with the X-ray photoelectron spectroscopy (XPS) results.

The transmission electron microscopy (TEM) images indicate, as shown in Figure 3a,b, that FeCo alloys, with a size of about 10 nm engrafted in graphitized poriferous carbon layers and CNTs, can be obviously observed. In particular, the FeCo alloy catalyzed the growth of CNTs, so that they were distributed on the surface of the graphitized porous carbon layers. It is also observed that the carbon nanotubes are wrapped with alloy nanoparticles at the ends. As presented in high-resolution transmission electron microscopy (HRTEM) (Figure 2c), the lattice spacing of 0.2 nm and 0.35 nm refer to the (110) and (002) planes of the FeCo alloy and graphitic carbon, respectively. The results reveal that FeCo alloy nanoparticles are encapsulated inside the graphitized carbon layer and construct a core–shell structure. The unique structure would be a benefit to good electromagnetic matching. In addition, a large number of bent CNT connections on the porous carbon surface form a conductive network. The clear lattice reveals that the FeCo alloy in FeCo/C–CNT nanocomposites has good crystallinity, which is in accordance with the XRD results. In addition, the diffraction planes of FeCo alloys were further confirmed by the diffraction rings obtained from the corresponding selected-area electron diffraction (SAED) pattern (Figure 3d). Consequently, FeCo/C–CNT nanocomposites derived from FeCo-ZIF MOFs were successfully synthesized, based on the above results.

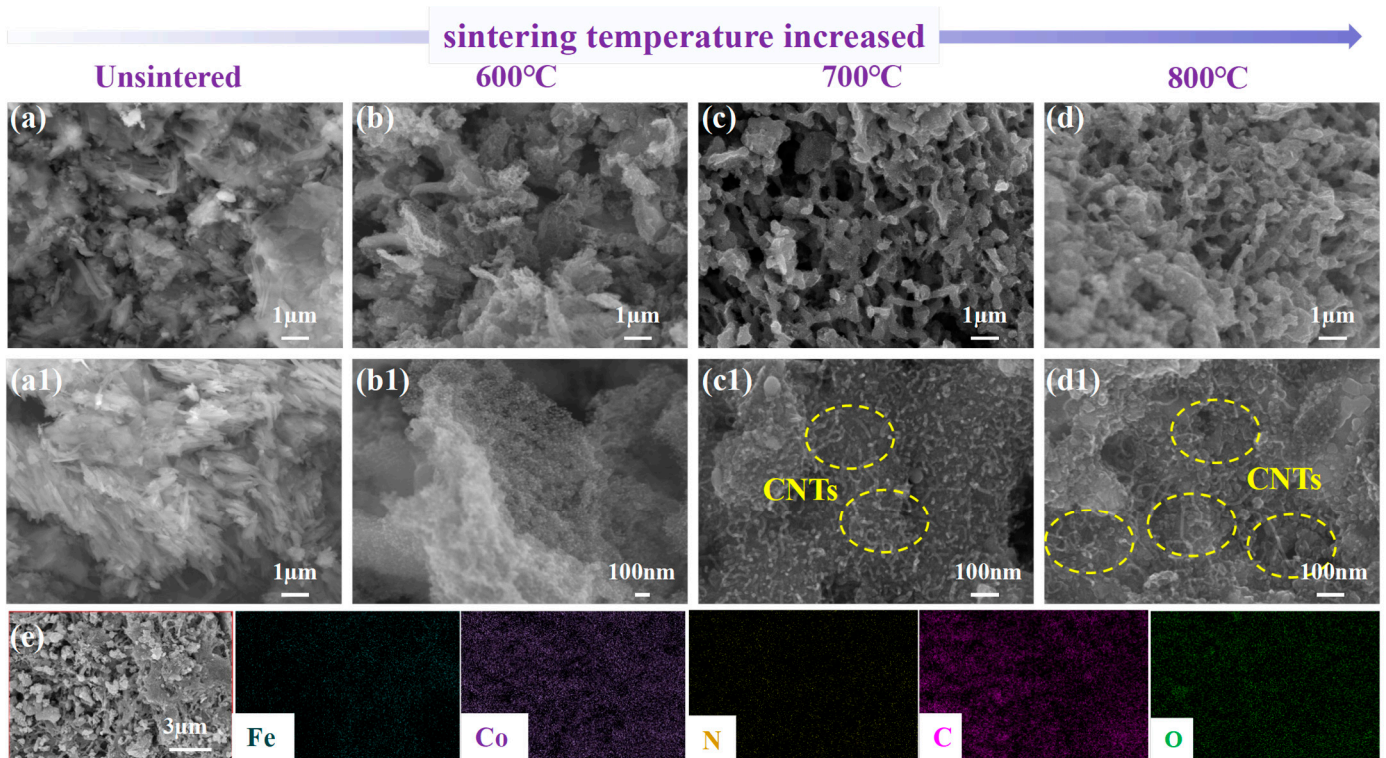


**Figure 2.** The scanning electron microscopy (SEM) images of (a,a1) FeCo-ZIF; (b,b1) FeCo/C-CNT-600; (c,c1) FeCo/C-CNT-700; (d,d1) FeCo/C-CNT-800; and (e) energy dispersive spectrometer (EDS) mapping of Fe, Co, N, C, and O elements.

Electromagnetic wave absorption performance can be deeply evaluated by analyzing the  $RL_{\min}$  values and EAB values, which are calculated according to the absorber thickness in the range of 1 to 6 mm in the frequency of 1–18 GHz [35,36]. Generally, the RL value is  $< -10$  dB, implying that approximately 90% of the electromagnetic energy is dissipated [37]. Figure 4 shows the 3D images of the RL values of the FeCo/C-CNT nanocomposites with different thicknesses. The detailed electromagnetic data, including the  $RL_{\min}$ , the frequency of the optimal RL, and the EAB are listed in Table 1. Both the pyrolysis temperature and the loading content in regard to the paraffin wax are essential for the EWA performance. In Figure 4a–c, the FeCo/C-CNT nanocomposites with a filling content of 20%, 30%, or 40%, under 600 °C sintering, all exhibit poor EWA ability. When increasing the calcination temperature, the  $RL_{\min}$  and EAB values remarkably improved. As shown in Figure 4e, the  $RL_{\min}$  of the FeCo/C-CNT-700-30 nanocomposite is  $-30.8$  dB at 9.6 GHz and the EAB reaches 11.42 GHz at 4.26 mm. Furthermore, the absorbing bandwidth of the FeCo/C-CNT-700-30 nanocomposite reaches 13.04 GHz (6.0 mm), nearly overlaying the whole C, X, and Ku band, which is far better than that of most absorbers. Notably, the EWA capabilities of FeCo/C-CNT nanocomposites under heat treatment at 800 °C are considerably improved. The  $RL_{\min}$  of the FeCo/C-CNT-800-20 nanocomposite reaches  $-52.06$  dB at 13.84 GHz and the EAB reaches 8.07 GHz at a thickness of 3.63 mm, as observed in Figure 4g.

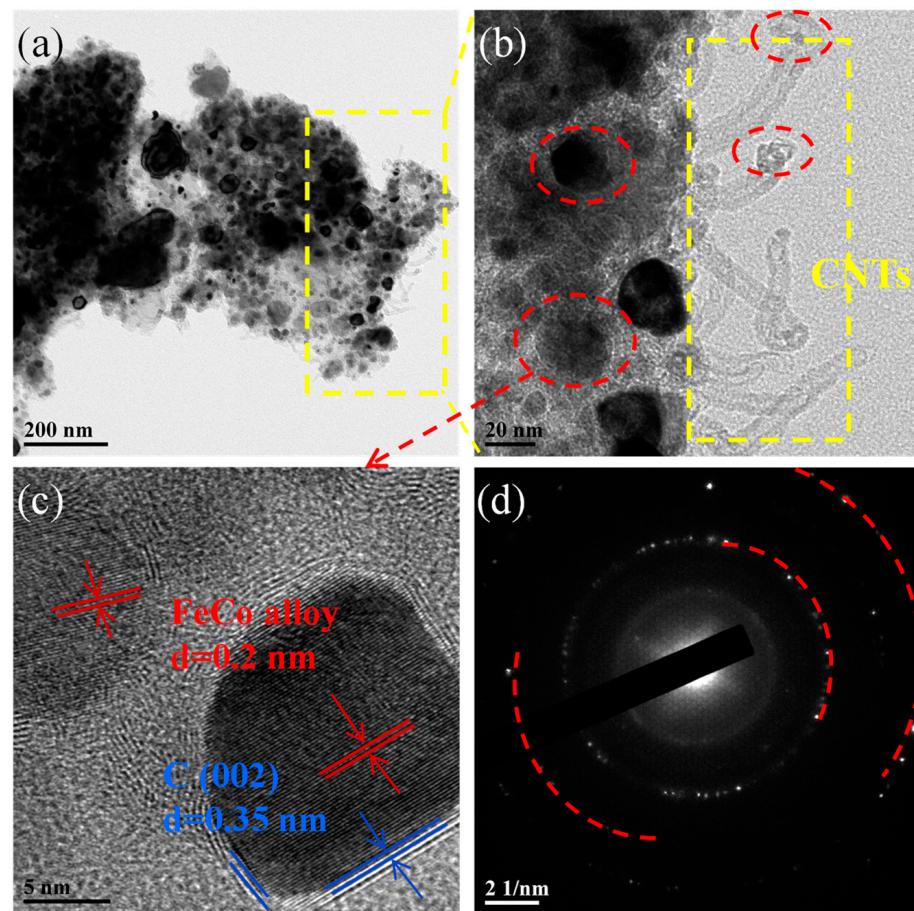


**Figure 3.** (a,b) The transmission electron microscopy (TEM) images, (c) high-resolution transmission electron microscopy (HRTEM) image, (d) selected-area electron diffraction (SAED) of FeCo/C–CNT-800 nanocomposite.

**Table 1.** Microwave absorption properties of FeCo/C–CNT nanocomposites.

Samples	RL <sub>min</sub> (dB)	Frequency (GHz)	EAB, RL < −10 dB	Thickness (mm)
FeCo/C–CNT-600-20	−6.85	7.7	\	4.5
FeCo/C–CNT-600-30	−9.26	2.78	\	5.0
FeCo/C–CNT-600-40	−9.23	2.89	\	5.0
FeCo/C–CNT-700-20	−9.79	15.14	\	2.5
FeCo/C–CNT-700-30	−30.8	9.6	11.42	4.26
	\	\	13.04	6.00
FeCo/C–CNT-700-40	−13.43	6.98	1.84	2.85
FeCo/C–CNT-800-20	−52.06	13.84	8.07	3.63
	−45.61	11.07	8.81	3.89
	\	\	9.80	5.00
FeCo/C–CNT-800-30	−60.26	15.94	4.95	1.86
	\	\	5.61	2.00
FeCo/C–CNT-800-40	−45.23	17.75	>3.96	1.28

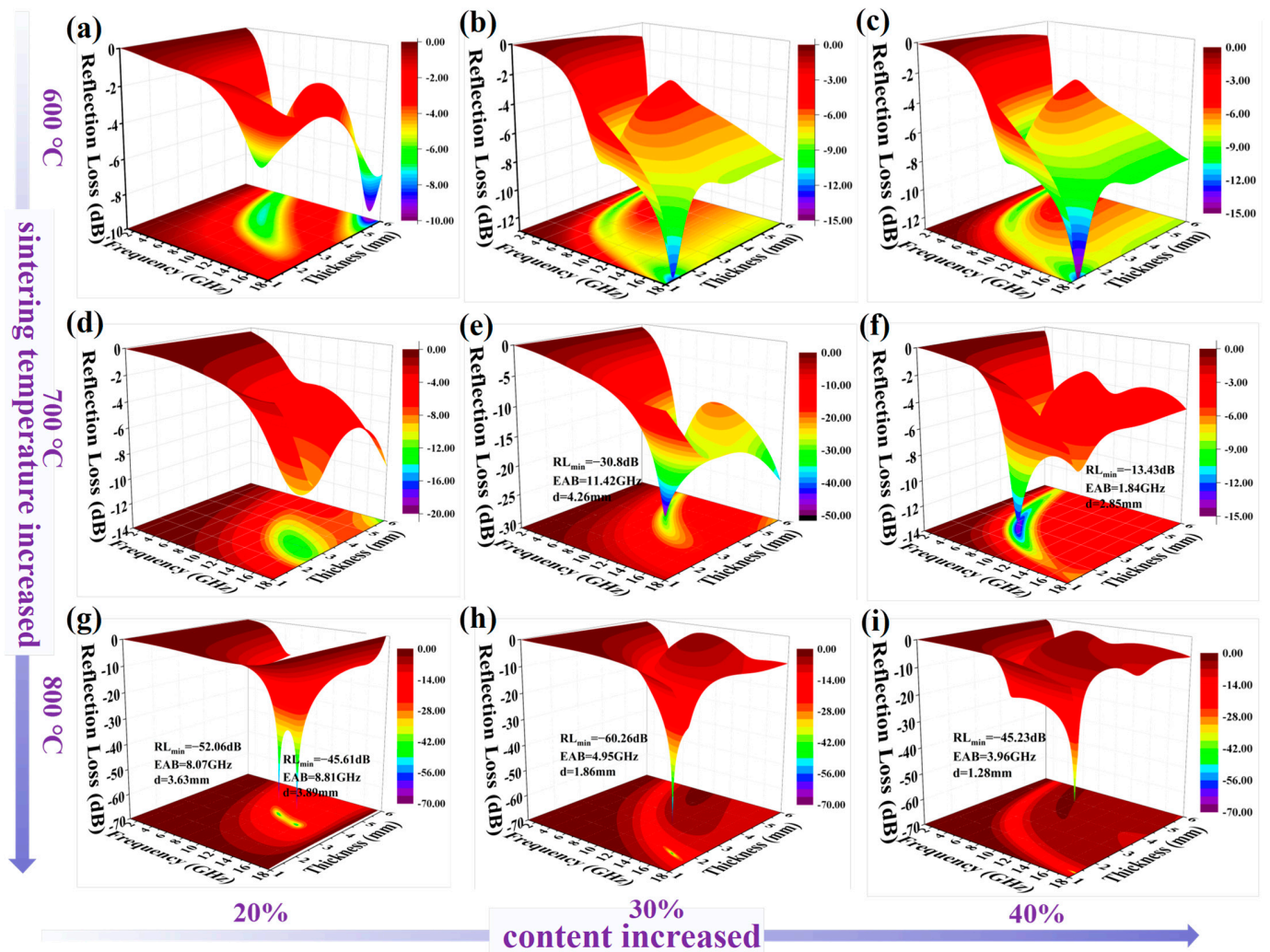


**Figure 4.** Numerous 3D representations of the reflection loss of (a) FeCo/C–CNT-600-20; (b) FeCo/C–CNT-600-30; (c) FeCo/C–CNT-600-40; (d) FeCo/C–CNT-700-20; (e) FeCo/C–CNT-700-30; (f) FeCo/C–CNT-700-40; (g) FeCo/C–CNT-800-20; (h) FeCo/C–CNT-800-30; and (i) FeCo/C–CNT-800-40 nanocomposites at different sintering temperatures with different wax filling content at 1–18 GHz.

Additionally, the  $RL_{\min}$  of the FeCo/C–CNT-800-20 nanocomposite is  $-45.61$  dB at  $3.89$  mm and the EAB value is  $8.81$  GHz. Along with the matching thickness of  $5$  mm, the absorption bandwidth increases to  $9.8$  GHz. When the filling content is  $30\%$  and the heat treatment temperature is  $800$  °C, FeCo/C–CNT-800-30 also displays good EWA effectiveness, with an  $RL_{\min}$  value of  $-60.26$  dB at  $15.94$  GHz, in terms of a thickness of  $1.86$  mm and an EAB of  $5.61$  GHz at  $2.0$  mm (Figure 4h). The results show that the pyrolysis temperature plays a significant role in the microwave absorption performance of FeCo/C–CNT nanocomposites. Meanwhile, it is found that the reflection losses are all increased when the filling is increased from  $20\%$  to  $30\%$ , and the reflection losses are all decreased when the filling is increased to  $40\%$ . While too high a filling will cause a higher dielectric loss, which makes the material impedance mismatch and leads to the degradation of the microwave absorption ability. As shown by previous SEM and TEM images, high crystallinity FeCo alloy nanoparticles are circumvented by the graphitized carbon layer and embedded into the end of the CNTs to form a porous structure, leading to good electric conductivity [25].

Further, to expand the practical application of FeCo/C–CNT nanocomposites, the materials were introduced into epoxy resin to construct a functional absorbing coating, whose reflectivity was studied using the arch test method, according to GJB539-2004.

Considering that the porous structure of cementitious composites may have multiple scattering and reflection effects on the EWA performance, ceramic brick was selected as a matrix to clarify the EWA ability of the epoxy resin coating decorated with FeCo/C–CNT nanocomposites. As shown in Figure 5, the minimum reflectivity of epoxy resin modified with 5 wt% FeCo/C–CNT nanocomposite is  $-23.89$  dB at  $11.37$  GHz, and the EAB reaches  $8.85$  GHz ( $2.36$ – $7.49$  GHz and  $8.55$ – $12.27$  GHz). The future looks bright for the obtained FeCo/C–CNT nanocomposites, which are expected to become exceptional EWA candidates as fillers for electromagnetic protection coatings in building applications.

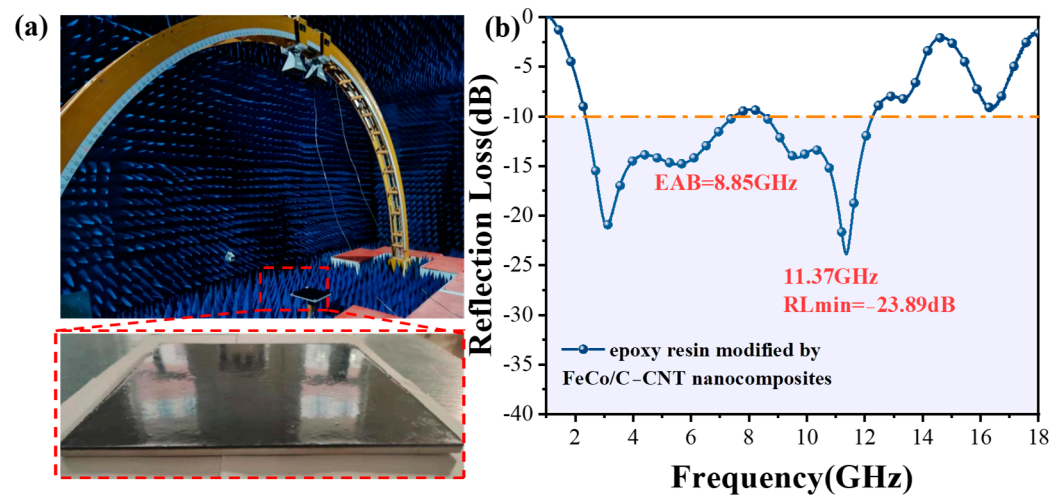


**Figure 5.** (a) The test procedure and a physical photograph and (b) RL curve of epoxy resin coating, modified with FeCo/C–CNT nanocomposites, on ceramic brick.

#### 4. Discussion

According to Figure 4, the FeCo/C–CNT-800-20 and FeCo/C–CNT-700-30 nanocomposites both have excellent reflection losses and wide effective bandwidths, which demonstrates that both the calcination temperature and the filling content are important in determining the EWA efficiency of nanocomposites. As the pyrolysis temperature increases, the reflection loss of FeCo/C–CNT nanocomposites increase at the same filling amount. A higher pyrolysis temperature occurs prior to growing more CNTs structures, which results in more conductive and interface polarization losses [38,39]. Impedance matching and a superior dissipation capability would be gained due to the magnetic–dielectric synergistic effect from the FeCo alloy, with ferromagnetic properties and graphitized carbon and CNTs providing the dielectric loss. Furthermore, abundant interfaces and holes are conducive to enhancing interfacial polarization and multiple microwave transmission paths, contributing to the absorption of electromagnetic waves. At the same pyrolysis temperature, the  $RL_{\min}$  values of FeCo/C–CNT nanocomposites show a tendency to increase and then decrease with the doping content increase in paraffin. This is due to the fact that the nanocomposite particles contact each other in the paraffin to form more conductive networks, resulting in a reflection loss increase. However, the excessive nanocomposites in the paraffin might obtain strong conductivity due to more contact from the conductive networks, causing an impedance mismatch, meaning that the incoming electromagnetic waves cannot enter the internal material. Thus, optimal FeCo/C–CNT nanocomposites not only improve the RL values, but also efficaciously widen the absorbing range, which have great potential as absorbing materials that meet the demand for practical applications.

It is common knowledge that that impedance matching is important for EWA efficiency, which is usually evaluated using impedance  $Z$  curves. The impedance  $Z$  curve vs the frequency can be calculated by Equation (3) [40,41]:

$$Z = \left| \frac{Z_{in}}{Z_0} \right| = \left( \frac{\mu_r}{\epsilon_r} \right)^{1/2} \tanh \left[ j \left( \frac{2\pi f d}{c} \right) (\mu_r \epsilon_r)^{1/2} \right] \quad (3)$$

Once the  $Z$  value approaches 1, it is demonstrated that more electromagnetic waves can enter the materials. As plotted in Figure 6e,g, two optimized samples exhibit outstanding impedance matching in a wide frequency range, resulting in a remarkable effective absorption band. In contrast, Figure 6a–d,f,h,i displays the  $Z$  values of other FeCo/C–CNT nanocomposites, where there is almost none close to 1, implying the poor impedance matching of the other composites.

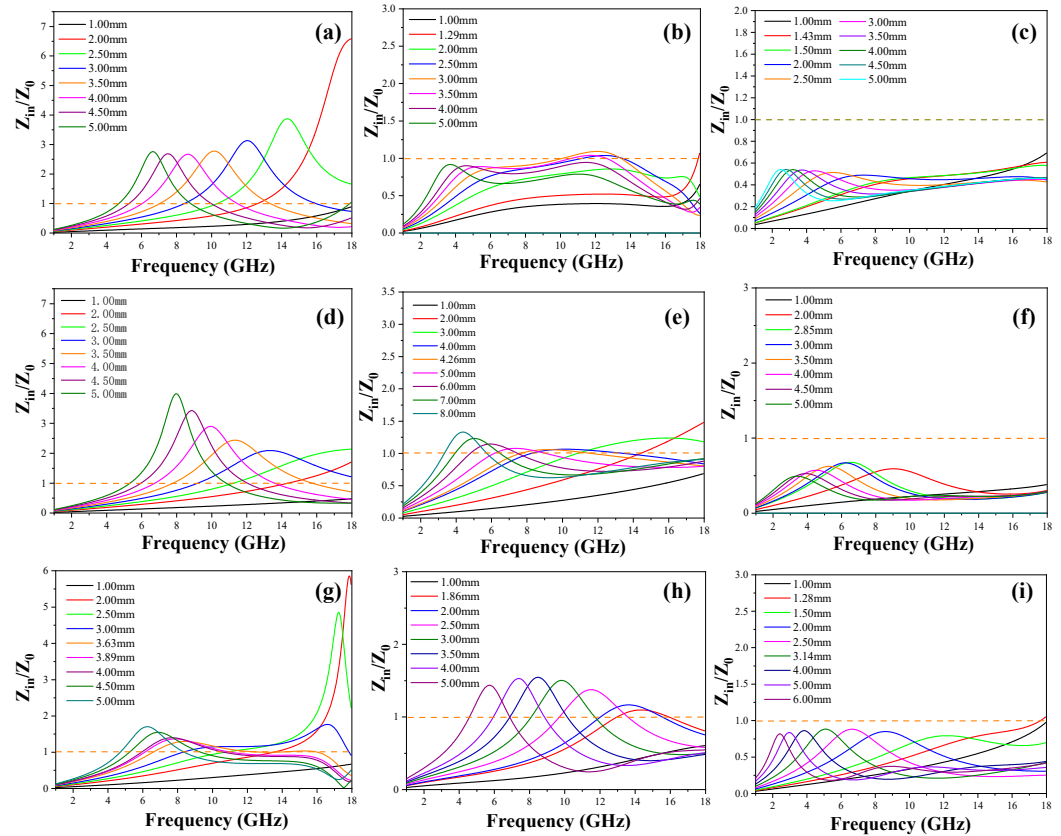


**Figure 6.** The impedance  $Z$  curves of (a) FeCo/C–CNT-600-20; (b) FeCo/C–CNT-600-30; (c) FeCo/C–CNT-600-40; (d) FeCo/C–CNT-700-20; (e) FeCo/C–CNT-700-30; (f) FeCo/C–CNT-700-40; (g) FeCo/C–CNT-800-20; (h) FeCo/C–CNT-800-30; and (i) FeCo/C–CNT-800-40 nanocomposites.

The electromagnetic absorption properties of FeCo/C–CNT nanocomposites can be analyzed using electromagnetic parameters. Moreover, the complex permittivity ( $\epsilon_r = \epsilon' - j\epsilon''$ ) and complex permeability ( $\mu_r = \mu' - j\mu''$ ) are presented in Figure 7 to assess the impacts of the calcination temperature and the filling content on the microwave absorption properties [42,43]. It is well known that the real parts of complex permittivity and complex permeability prove the storing ability of microwaves, as well as the imaginary parts of complex permittivity and complex permeability that designate the capability of dissipating microwaves [44,45]. As plotted in Figure 7a, the  $\epsilon'$  of FeCo/C–CNT nanocomposites decrease with frequency increases, exhibiting typical dispersive behavior. As seen in Figure 7b, the  $\epsilon''$  curve fluctuates, indicating that the composite has a polarization relaxation process. For the  $\mu''$  value, it has a higher value related to the imaginary part at 700 °C, indicating excellent magnetic loss. The lower  $\mu''$  value at 800 °C might originate from the graphitization degree increase in the non-magnetic porous carbon layer surrounding the FeCo alloy nanoparticles at high temperatures. Obviously, there is an absorption peak, which appeared at 13.04 GHz in the dielectric loss tangent ( $\tan\delta_\epsilon = \epsilon''/\epsilon'$ ) for FeCo/C–CNT-800, indicating more electromagnetic wave attenuation. It is demonstrated that a high pyrolysis temperature can generate more CNTs and high crystallinity of graphitic carbon, which would be favorable to enhancing electromagnetic energy loss and dielectric polarization. Nevertheless, as for complex permeability, FeCo/C–CNT-700 displays higher imaginary parts and

a higher tangent ( $\tan\delta_\mu = \mu''/\mu'$ ) of magnetic loss compared to that of FeCo/C–CNT-800, originating from the magnetic FeCo alloy components that are not completely coated by the carbon layers and CNTs.

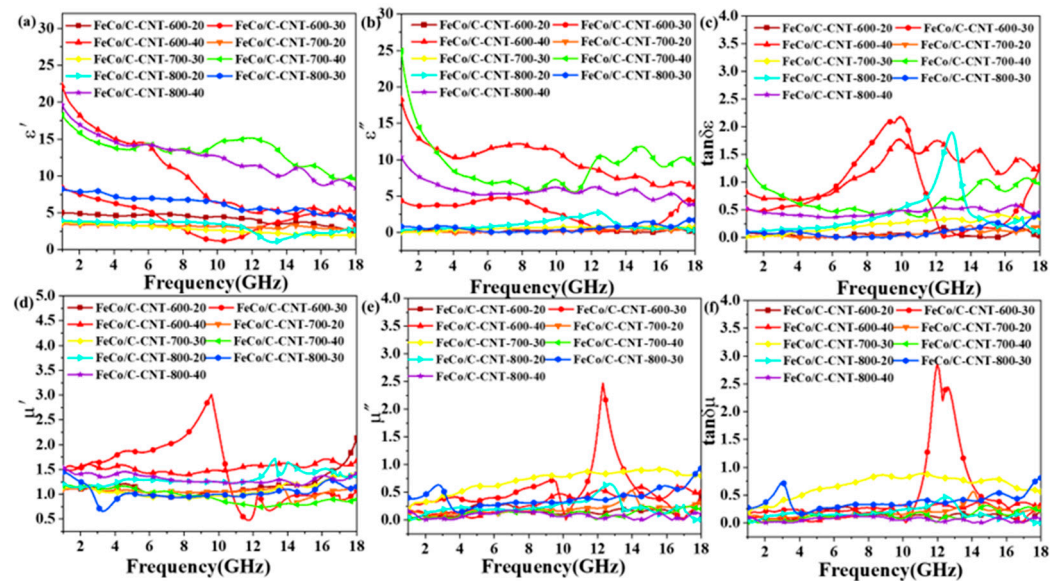


**Figure 7.** (a) Real part, (b) imaginary part of complex permittivity, (c) dielectric tangent loss values, (d) real part, (e) imaginary part of permeability, and (f) dielectric tangent loss values, for FeCo/C–CNT nanocomposites.

Furthermore, the Cole–Cole curves and attenuation constant were explored to access the microwave absorbing performance. The Cole–Cole curves are plotted by  $\epsilon'$  versus  $\epsilon''$ , as follows in the equation, according to Debye relaxation theory [46]:

$$\left(\epsilon' - \frac{\epsilon_s + \epsilon_\infty}{2}\right)^2 + (\epsilon'')^2 = \left(\frac{\epsilon_s - \epsilon_\infty}{2}\right)^2 \quad (4)$$

where  $\epsilon_s$  and  $\epsilon_\infty$  represent the static permittivity and relative permittivity at the high-frequency limit, respectively. One semicircle generally represents a Debye relaxation process. Figure 8 demonstrates that both FeCo/C–CNT-700 and FeCo/C–CNT-800 nanocomposites exhibit more semicircle numbers clearly than that of FeCo/C–CNT-600, proving that a high pyrolysis temperature helps to achieve the intense polarization relaxation and fantabulous dissipation ability.

Simultaneously, the microwave attenuation constant ( $\alpha$ ) can be derived from Equation (5) [47,48]:

$$\alpha = \frac{\sqrt{2\pi f}}{c} \times \sqrt{(\mu''\epsilon'' - \mu'\epsilon') + \sqrt{(\mu''\epsilon'' - \mu'\epsilon')^2 + (\epsilon'\mu'' + \epsilon''\mu')^2}} \quad (5)$$

As presented in Figure 9, the FeCo/C–CNT-600-40 nanocomposite possesses the biggest attenuation constant value compared to the other samples. However, the EWA performance of the FeCo/C–CNT-600-40 nanocomposite is not good, which might be attributed to poor impedance matching. Therefore, impedance matching is a more important factor in enhancing the microwave absorption efficiency than the attenuation loss in regard to our nanocomposites. Notably, FeCo/C–CNT-700 has a larger attenuation constant value than that of FeCo/C–CNT-800 in the frequency ranging from 1 to 18 GHz, implying that FeCo/C–CNT-700 has a better attenuation ability. In particular, the  $\alpha$  value of FeCo/C–CNT-800 decreases to zero from 17 GHz, which might result from the FeCo alloy embedding more CNTs and porous carbon layers, leading to weak magnetic loss in the high-frequency region. Based on the above results, the FeCo/C–CNT-700 and FeCo/C–

CNT-800 nanocomposites are the optimized candidates, with superior EWA capability, compared with the other samples.

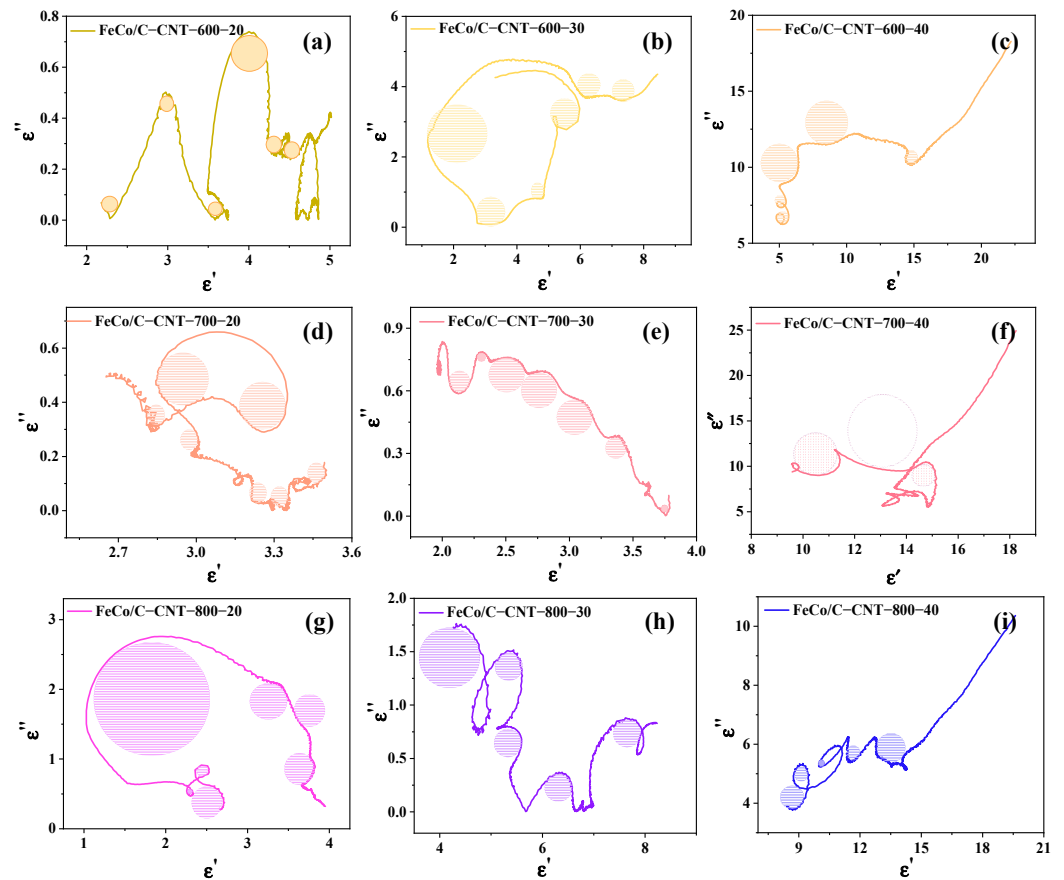


**Figure 8.** Cole–Cole plots of (a) FeCo/C–CNT-600-20; (b) FeCo/C–CNT-600-30; (c) FeCo/C–CNT-600-40; (d) FeCo/C–CNT-700-20; (e) FeCo/C–CNT-700-30; (f) FeCo/C–CNT-700-40; (g) FeCo/C–CNT-800-20; (h) FeCo/C–CNT-800-30; and (i) FeCo/C–CNT-800-40 nanocomposites.

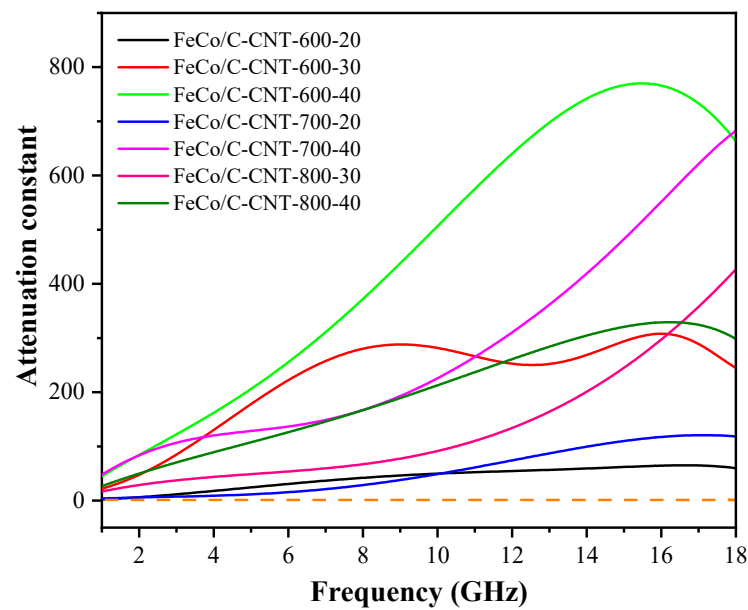


**Figure 9.** Attenuation constant  $\alpha$  of FeCo/C–CNT nanocomposites.

The enhancement mechanism of FeCo/C–CNT nanocomposites in regard to the wave absorption properties of epoxy resin is shown in Figure 10. Firstly, the magnetic–dielectric synergy effect from the FeCo alloy and carbon layers and CNTs results in outstanding impedance matching, which is beneficial for more microwaves to go into the interior of the absorbers. Simultaneously, electromagnetic waves would be dissipated by the magnetic loss from the FeCo alloy and the conductive loss originating from the carbon layers and CNTs. As well, the porous structures of nanocomposites are crucial in regard to the attenuation of microwaves, providing additional transmission paths for scattering and the reflection of electromagnetic waves, which results in the conversion of electromagnetic energy into other energy that dissipates. Undeniably, the existence of multiple interfaces among the FeCo alloy/carbon layers, FeCo alloy/CNTs, and carbon layers/CNTs would cause interface polarization, which is profitable to attenuate electromagnetic waves through the polarization relaxation process. Therefore, the impedance matching, double loss mechanisms, conductive loss, multiple reflection, and polarization effects of FeCo/C–CNT nanoscale wave absorbers enable the modified epoxy coating to have an ultrabroad EAB, exhibit significant EWA performance, and provide a brand new way of thinking for the application of EWA coatings.

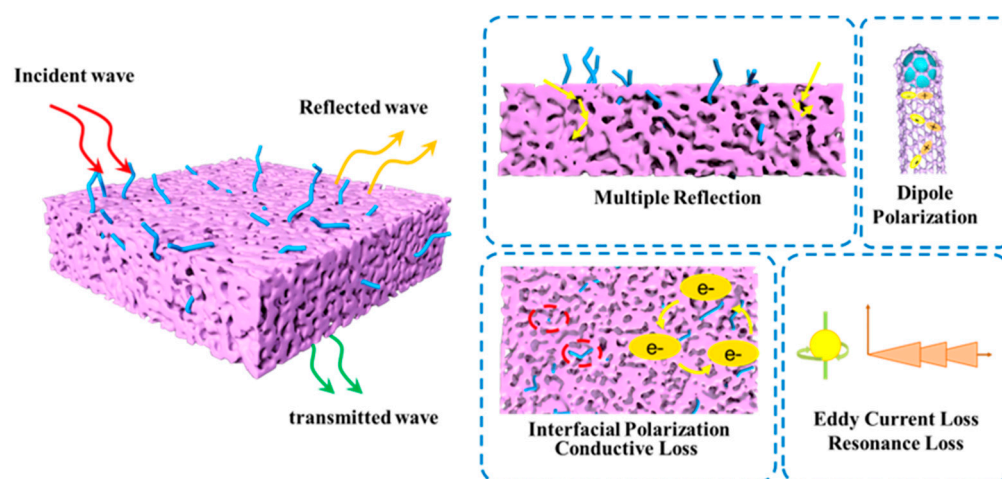


**Figure 10.** Possible electromagnetic microwave attenuation mechanisms of FeCo/C–CNT nanocomposites in epoxy resin.

## 5. Conclusions

In summary, FeCo/C–CNT nanocomposites were successfully synthesized through simple pyrolysis of FeCo-ZIF precursors. Based on their excellent microwave absorption properties, a novel EWA coating was prepared using them as absorber fillers and epoxy resin as a binder. The excellent impedance matching characteristics, magnetic–dielectric synergistic effect, interfacial polarization effect, and multiple scattering and reflection inside the FeCo/C–CNT nanocomposites endow the epoxy resin coating with an ultra-wideband EWA performance. The coating has a minimum reflectivity of  $-23.89$  dB at 11.37 GHz and absorbs more than 90% of electromagnetic waves in the frequency ranges 2.36–7.49 GHz and 8.55–12.27 GHz. This study has successfully developed an EWA coating for the surface of ceramic tile construction materials and provided a new idea to enhance the application potential of epoxy resin and reduce electromagnetic pollution.

**Author Contributions:** Conceptualization, Y.L.; methodology, J.L., C.L. and C.D.; validation, J.L. and C.L.; investigation, D.L., J.L., D.Y., J.Z., F.H. and Z.G.; resources, Y.L.; writing—original draft preparation, D.L. and J.L.; writing—review and editing, Y.L.; supervision, Y.L.; funding acquisition, D.L. All authors have read and agreed to the published version of the manuscript.

**Funding:** This work was funded by the Qingchuang Technology Project under Grant 2021KJ045. Thanks are given to the Joint Funds of the National Natural Science Foundation of China (U22A20244, U23A20673) and the National Natural Science Foundation of China (NSFC, Grant No. 52002201). Qingdao West Coast New Area 2022, 2021 Science and Technology Plan Special Project (2022-41, 2021-102) are also acknowledged.

**Data Availability Statement:** The data is contained within the article: The original contributions presented in the study are included in the article, further inquiries can be directed to the corresponding author.

**Acknowledgments:** This work was supported by the School of Civil Engineering, Qingdao University of Technology.

**Conflicts of Interest:** Donglei Yang was employed by Institute of Technical Information for Building Materials Industry. Jiqing Zhang was employed by Qingdao Ruiyuan Engineering Group Co., Ltd.; Feizi Han was employed by CIECC Overseas Consulting Co., Ltd. The remaining authors declare that the research was conducted in the absence of any commercial or financial relationships that could be construed as a potential conflict of interest.

## References

1. Wen, B.; Yang, H.B.; Lin, Y.; Qiu, Y.; Cheng, Y.; Jin, L.X. Novel bimetallic MOF derived hierarchical Co@C composites modified with carbon nanotubes and its excellent electromagnetic wave absorption properties. *J. Colloid Interface Sci.* **2022**, *605*, 657–666. [[CrossRef](#)]
2. Qiu, Y.; Lin, Y.; Yang, H.B.; Wang, L.; Wang, M.Q.; Wen, B. Hollow Ni/C microspheres derived from Ni-metal organic framework for electromagnetic wave absorption. *Chem. Eng. J.* **2020**, *383*, 123207. [[CrossRef](#)]
3. Xu, X.Q.; Li, D.S.; Li, L.; Yang, Z.; Lei, Z.Q.; Xu, Y.X. Architectural design and microstructural engineering of metal-organic framework-derived nanomaterials for electromagnetic wave absorption. *Small Struct.* **2022**, *4*, 2200219. [[CrossRef](#)]
4. Zhao, S.X.; Ma, H.; Shao, T.Q.; Wang, J.; Yang, Z.N.; Meng, Y.Y.; Feng, M.D.; Yan, M.B.; Wang, J.F.; Qu, S.B. High temperature metamaterial enhanced electromagnetic absorbing coating prepared with alumina ceramic. *J. Alloys Compd.* **2021**, *874*, 159822. [[CrossRef](#)]
5. Li, X.; Zhou, Q.H.; Huang, Y.Y.; Yang, J.P. Nanoindentation and abrasion in Fe<sub>3</sub>O<sub>4</sub>/rGO reinforced epoxy electromagnetic protective coatings. *J. Alloys Compd.* **2021**, *887*, 161277. [[CrossRef](#)]
6. Shao, T.Q.; Ma, H.; Wang, J.; Feng, M.D.; Yan, M.B.; Wang, J.F.; Yang, Z.N.; Zhou, Q.; Luo, H.; Qu, S.B. High temperature absorbing coatings with excellent performance combined Al<sub>2</sub>O<sub>3</sub> and TiC material. *J. Eur. Ceram. Soc.* **2020**, *40*, 2013–2019. [[CrossRef](#)]
7. Sun, T.P.; Liu, Z.W.; Li, S.; Liu, H.S.; Chen, F.; Wang, K.; Zhao, Y. Effective improvement on microwave absorbing performance of epoxy resin-based composites with 3D MXene foam prepared by one-step impregnation method. *Compos. Part A* **2021**, *150*, 106594. [[CrossRef](#)]
8. Li, R.; Qing, Y.C.; Li, W.; Li, Y. The electromagnetic absorbing properties of plasma-sprayed TiC/Al<sub>2</sub>O<sub>3</sub> coatings under oblique incident microwave irradiation. *Ceram. Int.* **2021**, *47*, 22864–22868. [[CrossRef](#)]
9. Xia, Y.X.; Gao, W.W.; Gao, C. A review on graphene-based electromagnetic functional materials: Electromagnetic wave shielding and absorption. *Adv. Funct. Mater.* **2022**, *32*, 2204591. [[CrossRef](#)]
10. Du, B.; Cai, M.; Wang, X.; Qian, J.J.; He, C.; Shui, A.Z. Enhanced electromagnetic wave absorption property of binary ZnO/NiCo<sub>2</sub>O<sub>4</sub> composites. *J. Adv. Ceram.* **2021**, *10*, 832–842. [[CrossRef](#)]
11. Zheng, T.T.; Zhang, Y.; Jia, Z.R.; Zhu, J.H.; Wu, G.L.; Yin, P.F. Customized dielectric-magnetic balance enhanced electromagnetic wave absorption performance in Cu<sub>x</sub>S/CoFe<sub>2</sub>O<sub>4</sub> composites. *Chem. Eng. J.* **2022**, *457*, 140876. [[CrossRef](#)]
12. Liu, C.; Wang, J.; Wan, J.; Yu, C.Z. MOF-on-MOF hybrids: Synthesis and applications. *Coord. Chem. Rev.* **2021**, *432*, 213743. [[CrossRef](#)]
13. Chai, L.L.; Pan, J.Q.; Hu, Y.; Qian, J.; Hong, M.C. Rational design and growth of MOF-on-MOF heterostructures. *Small* **2021**, *17*, 2100607. [[CrossRef](#)] [[PubMed](#)]
14. Ye, Z.Q.; Jiang, Y.; Li, L.; Wu, F.; Chen, R.J. Rational design of MOF-based materials for next-generation rechargeable batteries. *Nano-Micro Lett.* **2021**, *13*, 203. [[CrossRef](#)] [[PubMed](#)]
15. Mai, C.W.; Huang, N.N.; Gao, M.Y.; Sun, Y.S.; Yan, J.F.; Zhai, C.X.; Zhao, W. Natural green raw-based Biochar@Co/C composites: Simple water bath synthesis and excellent electromagnetic wave absorption properties. *J. Alloys Compd.* **2023**, *968*, 171960. [[CrossRef](#)]
16. Zhang, F.; Yin, S.Y.; Chen, Y.F.; Zheng, Q.; Wang, L.J.; Jiang, W. Ligand-directed construction of CNTs-decorated metal carbide/carbon composites for ultra-strong and broad electromagnetic wave absorption. *Chem. Eng. J.* **2022**, *433*, 133586. [[CrossRef](#)]
17. Gao, Z.G.; Iqbal, A.; Hassan, T.; Zhang, L.M.; Wu, H.J.; Koo, C.M. Texture regulation of metal-organic frameworks, microwave absorption mechanism-oriented structural optimization and design perspectives. *Adv. Sci.* **2022**, *9*, 2204151. [[CrossRef](#)] [[PubMed](#)]

18. Panahi-Sarmad, M.; Samsami, S.; Ghaffarkhah, A.; Hashemi, S.A.; Ghasemi, S.; Amini, M.; Wuttke, S.; Rojas, O.; Tam, K.C.; Jiang, F.; et al. MOF-based electromagnetic shields multiscale design: Nanoscale chemistry, microscale assembly, and macroscale manufacturing. *Adv. Funct. Mater.* **2023**, 2304473. [[CrossRef](#)]
19. Lan, Q.; Shan, L. MOF derived porous Ni/Co@C nanocomposite as electromagnetic wave absorber with optimized impedance matching. *Compos. Commun.* **2022**, 33, 101196.
20. Qin, L.; Liu, S.; Qin, S.H.; Liao, L.F.; He, M.; Yu, J. Efficient and lightweight electromagnetic wave absorber derived from metal organic framework-encapsulated cobalt nanoparticles. *ACS Appl. Mater. Interfaces* **2017**, 9, 42102–42110.
21. Lu, C.X.; Geng, H.R.; Zhu, Y.B.; Ma, J.M.; Wang, R.W.; Liu, X.F.; Tu, G.L. 3D flower-shape Co/Cu bimetallic nanocomposites with excellent wideband electromagnetic microwave absorption. *Appl. Surf. Sci.* **2023**, 615, 156219. [[CrossRef](#)]
22. Qiang, R.; Du, Y.C.; Zhao, H.T.; Wang, Y.; Tian, C.H.; Li, Z.G.; Han, X.J.; Xu, P. Metal organic framework-derived Fe/C nanocubes toward efficient microwave absorption. *J. Mater. Chem. A* **2015**, 3, 13426–13434. [[CrossRef](#)]
23. Wu, Q.; Wang, B.L.; Fu, Y.G.; Zhang, Z.F.; Yan, P.F.; Liu, T. MOF-derived Co/CoO particles prepared by low temperature reduction for microwave absorption. *Chem. Eng. J.* **2021**, 410, 128378. [[CrossRef](#)]
24. Lu, Y.Y.; Wang, Y.T.; Li, H.L.; Lin, Y.; Jiang, Z.Y.; Xie, Z.X.; Kuang, Q.; Zheng, L.S. MOF-derived porous Co/C nanocomposites with excellent electromagnetic wave absorption properties. *ACS Appl. Mater. Interfaces* **2015**, 7, 13604–13611. [[CrossRef](#)] [[PubMed](#)]
25. Zhang, F.; Jia, Z.R.; Zhou, J.X.; Liu, J.K.; Wu, G.L.; Yin, P.F. Metal-organic framework-derived carbon nanotubes for broadband electromagnetic wave absorption. *Chem. Eng. J.* **2022**, 450, 138205. [[CrossRef](#)]
26. Guo, S.Y.; Bao, Y.F.; Li, Y.; Guan, H.L.; Lei, D.Y.; Zhao, T.J.; Zhong, B.M.; Li, Z.H. Super broadband absorbing hierarchical CoFe alloy/porous carbon@carbon nanotubes nanocomposites derived from metal-organic frameworks. *J. Mater. Sci. Technol.* **2022**, 118, 218–228. [[CrossRef](#)]
27. Li, X.; Huang, C.; Wang, Z.L.; Xiang, Z.; Lu, W. Enhanced electromagnetic wave absorption of layered FeCo@carbon nanocomposites with a low filler loading. *J. Alloys Compd.* **2021**, 879, 160465. [[CrossRef](#)]
28. Zhang, X.F.; Li, Y.X.; Liu, R.G.; Rao, Y.; Rong, H.W.; Qin, G.W. High-magnetization FeCo nanochains with ultrathin interfacial gaps for broadband electromagnetic wave absorption at gigahertz. *ACS Appl. Mater. Interfaces* **2016**, 8, 3494–3498. [[CrossRef](#)] [[PubMed](#)]
29. Wang, S.S.; Xu, Y.C.; Fu, R.R.; Zhu, H.H.; Jiao, Q.Z.; Feng, T.Y.; Feng, C.H.; Shi, D.X.; Li, H.S.; Zhao, Y. Rational construction of hierarchically porous Fe-Co/N-doped carbon/rGO composites for broadband microwave absorption. *Nano-Micro Lett.* **2019**, 11, 76. [[CrossRef](#)]
30. Bao, Y.; Guo, R.Y.; Liu, C.; Li, S.; Ma, J.Z. Design of magnetic triple-shell hollow structural Fe<sub>3</sub>O<sub>4</sub>/FeCo/C composite microspheres with broad bandwidth and excellent electromagnetic wave absorption performance. *Ceram. Int.* **2020**, 46, 23932–23940. [[CrossRef](#)]
31. Xiong, Y.; Xu, L.L.; Yang, C.X.; Sun, Q.F.; Xu, X.J. Implanting FeCo/C nanocages with tunable electromagnetic parameters in anisotropic wood carbon aerogels for efficient microwave absorption. *J. Mater. Chem. A* **2020**, 8, 18863–18871. [[CrossRef](#)]
32. Shen, Z.J.; Yang, H.L.; Liu, C.B.; Guo, E.W.; Huang, S.Y.; Xiong, Z.Q. Polymetallic MOF-derived corn-like composites for magnetic-dielectric balance to facilitate broadband electromagnetic wave absorption. *Carbon* **2021**, 185, 464–476. [[CrossRef](#)]
33. Zhang, X.M.; Xian, G.Y.; Wang, J.Y.; Fan, Y.; Liu, Y.; Oh, W.C.; Liu, Z.Y.; Wang, Y.Q.; Kong, L.B. Evolution of hollow dodecahedron carbon coated FeCo with enhance of electromagnetic properties. *Adv. Powder Technol.* **2022**, 33, 103854. [[CrossRef](#)]
34. Zhao, H.Q.; Jin, C.Q.; Yang, X.; Lu, P.; Cheng, Y. Synthesis of a one-dimensional carbon nanotube-decorated three-dimensional crucifix carbon architecture embedded with Co<sub>7</sub>Fe<sub>3</sub>/Co<sub>5.47</sub>N nanoparticles for high-performance microwave absorption. *J. Colloid Interface Sci.* **2023**, 645, 22–32. [[CrossRef](#)]
35. Qiao, J.; Zhang, X.; Liu, C.; Lyu, L.F.; Yang, Y.F.; Wang, Z.; Wu, L.L.; Liu, W.; Wang, F.L.; Liu, J.R. Non-magnetic bimetallic MOF-derived porous carbon-wrapped TiO<sub>2</sub>/ZrTiO<sub>4</sub> composites for efficient electromagnetic wave absorption. *Nano-Micro Lett.* **2021**, 13, 75. [[CrossRef](#)]
36. Zhang, S.J.; Cheng, B.; Jia, Z.R.; Zhao, Z.W.; Jin, X.T.; Zhao, Z.H.; Wu, G.L. The art of framework construction: Hollow-structured materials toward high-efficiency electromagnetic wave absorption. *Adv. Compos. Hybrid Mater.* **2022**, 5, 1658–1698. [[CrossRef](#)]
37. Liu, Y.; Zhou, X.F.; Jia, Z.R.; Wu, H.J.; Wu, G.L. Oxygen vacancy-induced dielectric polarization prevails in the electromagnetic wave-absorbing mechanism for Mn-based MOFs-derived composites. *Adv. Funct. Mater.* **2022**, 32, 2204499. [[CrossRef](#)]
38. Yang, M.L.; Yuan, Y.; Li, Y.; Sun, X.X.; Wang, S.S.; Liang, L.; Ning, Y.H.; Li, J.J.; Yin, W.L.; Che, R.C.; et al. Dramatically enhanced electromagnetic wave absorption of hierarchical CNT/Co/C fiber derived from cotton and metal-organic-framework. *Carbon* **2020**, 161, 517–527. [[CrossRef](#)]
39. Yan, J.; Huang, Y.; Han, X.P.; Gao, X.G.; Liu, P.B. Metal organic framework (ZIF-67)-derived hollow CoS<sub>2</sub>/N-doped carbon nanotube composites for extraordinary electromagnetic wave absorption. *Compos. Part B Eng.* **2019**, 163, 67–76. [[CrossRef](#)]
40. Wang, K.F.; Chen, Y.J.; Tian, R.; Li, H.; Zhou, Y.; Duan, H.N.; Liu, H.Z. Porous Co-C core-shell nanocomposites derived from Co-MOF-74 with enhanced electromagnetic wave absorption performance. *ACS Appl. Mater. Interfaces* **2018**, 10, 11333–11342. [[CrossRef](#)]
41. Wang, L.; Huang, M.Q.; Yu, X.F.; You, W.B.; Zhang, J.; Liu, X.H.; Wang, M.; Che, R.C. MOF-Derived Ni<sub>1-x</sub>Co<sub>x</sub>@Carbon with tunable nano-microstructure as lightweight and highly efficient electromagnetic wave absorber. *Nano-Micro Lett.* **2020**, 12, 150. [[CrossRef](#)] [[PubMed](#)]
42. Huang, X.M.; Liu, X.H.; Jia, Z.R.; Wang, B.B.; Wu, X.M.; Wu, G.L. Synthesis of 3D cerium oxide/porous carbon for enhanced electromagnetic wave absorption performance. *Adv. Compos. Hybrid Mater.* **2021**, 4, 1398–1412. [[CrossRef](#)]

43. Yang, B.T.; Fang, J.F.; Xu, C.Y.; Cao, H.; Zhang, R.X.; Zhao, B.A.; Huang, M.Q.; Wang, X.Y.; Lv, H.L.; Che, R.C. One-dimensional magnetic FeCoNi alloy toward low-frequency electromagnetic wave absorption. *Nano-Micro Lett.* **2022**, *14*, 170. [[CrossRef](#)] [[PubMed](#)]
44. Zhang, F.; Cui, W.; Wang, B.B.; Xu, B.H.; Liu, X.H.; Liu, X.H.; Jia, Z.R.; Wu, G.L. Morphology-control synthesis of polyaniline decorative porous carbon with remarkable electromagnetic wave absorption capabilities. *Compos. Part B Eng.* **2021**, *204*, 108491. [[CrossRef](#)]
45. Wu, Z.C.; Cheng, H.W.; Jin, C.; Yang, B.; Xu, C.Y.; Pei, K.; Zhang, H.B.; Yang, Z.Q.; Che, R.C. Dimensional design and core-shell engineering of nanomaterials for electromagnetic wave absorption. *Adv. Mater.* **2022**, *34*, 2107538. [[CrossRef](#)] [[PubMed](#)]
46. Jia, Z.R.; Zhang, X.Y.; Gu, Z.; Wu, G.L. MOF-derived Ni-Co bimetal/porous carbon composites as electromagnetic wave absorber. *Adv. Compos. Hybrid Mater.* **2023**, *6*, 28. [[CrossRef](#)]
47. Song, L.M.; Zhang, F.; Chen, Y.Q.; Guan, L.; Zhu, Y.Q.; Chen, M.; Wang, H.L.; Putra, B.R.; Zhang, R.; Fan, B.B. Multifunctional SiC@SiO<sub>2</sub> nanofiber aerogel with ultrabroadband electromagnetic wave absorption. *Nano-Micro Lett.* **2022**, *14*, 152. [[CrossRef](#)]
48. Ma, M.L.; Liao, Z.J.; Su, X.W.; Zheng, Q.X.; Liu, Y.Y.; Wang, Y.; Ma, Y.; Wan, F. Magnetic CoNi alloy particles embedded N-doped carbon fibers with polypyrrole for excellent electromagnetic wave absorption. *J. Colloid Interface Sci.* **2022**, *608*, 2203–2212. [[CrossRef](#)]

**Disclaimer/Publisher's Note:** The statements, opinions and data contained in all publications are solely those of the individual author(s) and contributor(s) and not of MDPI and/or the editor(s). MDPI and/or the editor(s) disclaim responsibility for any injury to people or property resulting from any ideas, methods, instructions or products referred to in the content.